Design of a New Mimochrome with Unique Topology

Angela Lombardi,[a] Flavia Nastri,[a] Daniela Marasco,[a] Ornella Maglio,[a, d] Giampiero De Sanctis,[b] Federica Sinibaldi,[c] Roberto Santucci,[c] Massimo Coletta,[c] and Vincenzo Pavone*[a]

Abstract: Peptide-based metalloprotein models represent useful systems to help understand how metalloproteins can support different functions, by the use of similar metal ion cofactors. In order to shed light on the role of the protein matrix in modulating the heme properties, we developed new models: mimochromes. They are pseudo-C_2 symmetric systems, composed of two helical peptides covalently linked to the deuteroporphyrin. The use of C_2 symmetry is particularly advantageous, because it simplifies the design, synthesis and characterization. However, it leaves the problem of possible diastereomeric forms. In the cobalt complex of the first derivative, mimochrome I, Λ and Δ isomers were indeed experimentally observed. All the insights derived from the Co^{III}–mimochrome I structure were used to obtain a re-designed molecule, mimochrome IV. The spectroscopic characterization of the iron and cobalt derivatives suggested the presence of the Λ isomer as unique species. The NMR solution structure of the diamagnetic Co^{III}–mimochrome IV confirmed the ability of the molecule to adopt a unique topology, and revealed the peptide chains to be in helical conformation, as designed. The insertion of intramolecular, inter-chain interactions was successful in favoring the formation of one of the two possible diastereomers. The stereochemically stable structure of mimochrome IV provides an attractive model for modulating the redox potential of the heme, by simple changing the peptide chain composition around the heme.

Keywords: helical structures · heme proteins · miniaturized metalloproteins · NMR spectroscopy · protein design

Introduction

Metals in biology perform a variety of important chemical transformations, and it is still an open question how basic recurrent metal sites can effect diverse functions.[1] This feature is strictly related to the protein matrix that dictates the hydrophobicity, the charge distribution, the nature of coordinating residues, and the polarity of the environment around the metal center.

The search for artificial catalytic systems able to reproduce the properties of natural metalloenzymes is a key field in bioinorganic chemistry.[2] Recently, the use of peptides has emerged as an efficient tool for reproducing metalloenzyme active sites.[3] We have approached the challenge of accessing metalloprotein models using a miniaturization process. We have successfully applied this approach to the development of miniaturized heme and non-heme iron-containing metalloproteins,[4–6] and we report here the results on mimochrome IV, a miniaturized heme protein.

Mimochromes are peptide–porphyrin conjugates with a pseudo-C_2 symmetry. They consist of deuteroporphyrin, covalently linked to two peptides (nine or fourteen residues), via an amide bond between the porphyrin propionyl groups and the side chains of two Lys residues.[5] Figure 1 reports a

[a] Prof. V. Pavone, Prof. A. Lombardi, Dr. F. Nastri, Dr. D. Marasco, Dr. O. Maglio
University of Napoli Federico II
Department of Chemistry
Complesso Universitario Monte S. Angelo
Via Cynthia, 80126 Napoli (Italy)
Fax: (+39) 081-674-090
E-mail: pavone@chemistry.unina.it

[b] Prof. G. De Sanctis
Department of Molecular, Cellular and Animal Biology
University of Camerino
Via F. Camerini 2, 62032 Camerino (MC) (Italy)

[c] Dr. F. Sinibaldi, Prof. R. Santucci, Prof. M. Coletta
Department of Experimental Medicine and Biochemical Sciences
University of Roma Tor Vergata
Via di Tor Vergata 135, 00133 Roma (Italy)

[d] Dr. O. Maglio
Permanent address: Istituto di Biostrutture e Bioimmagini - C.N.R.
via Mezzocannone 6, 80134 Napoli (Italy)

Supporting information for this article is available on the WWW under http://www.chemeurj.org/ or from the author: ^{1}H NMR (1D and 2D-NOESY) spectra of Co^{III}–mimochrome IV, and UV/Vis spectrum of Fe^{III}–mimochrome IV at pH 9.5, with chemical shift data, coupling constants and hydrogen bonds. Atomic coordinates have been deposited within the Protein Data Bank (pdb code: 1 L1B).

 DOI: 10.1002/chem.200304831

schematic representation of mimochromes. The peptide fragments (residues 1–9), which face the porphyrin plane, are in α-helical conformation, a common feature of several natural heme proteins. The α-helix is a well-defined rigid scaffold, which can accommodate several amino acid substitutions without severe structural perturbations; therefore, numerous model compounds, based on helical peptides, have been developed (for recent reviews see ref. [3e,4]). The peptide sandwiched mesoheme,[7] the disulfide linked α-helices–monoheme adducts,[8] the MOP derivatives,[9] and the heme maquettes[10] are examples of either covalent or non-covalent artificial heme-peptide conjugates.

Among the mimochrome class of artificial heme proteins, the prototype member, mimochrome I, was designed with the aim of finding the smallest peptide sequence able to fold into α-helical conformation and to coat the heme group completely.[5a] It contains two identical N- and C-terminal protected nonapeptides, each bearing a His residue in the central position, which acts as axial ligand to the central iron ion.

The fully characterization of mimochrome I iron and cobalt complexes confirmed the design, even though some unexpected features were observed. The iron complex showed quite low solubility in water (in the μM range), in a wide range of experimental conditions.[5a,c] Its detailed characterization was henceforth strongly limited. On the opposite, the cobalt complex was soluble in water (up to mM concentration), but two equally abundant isomers were obtained (see Figure 2). Because of the flexibility of the linker between the peptide and the deuteroporphyrin ring, each peptide chain can be positioned either above or below the porphyrin plane, giving rise to Δ and Λ diastereomers (see Figure 2a and b), which were structurally characterized in solution by NMR (Figure 2c).[5b]

As an important result, both diastereomers are stable and clearly distinguishable, even at very acidic conditions (pH <1), because the cobalt–histidine coordination is strong enough to preserve the sandwich structure. On the opposite, the iron complex is exchange-labile and a fast interconversion between the two diastereomeric forms occurs. During the interconversion process both peptide chains must move from one face of the porphyrin to the other, and the porphyrin ring becomes exposed to the solvent. Henceforth, aggregation by stacking of the porphyrin ring may occur, and low water solubility of Fe^{III}–mimochrome I is observed.

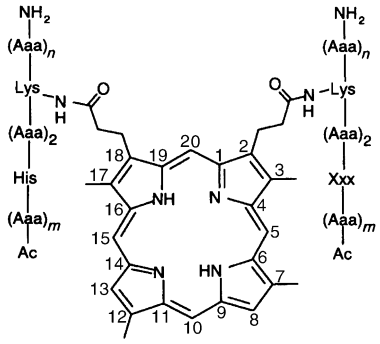

Derivative	*n*	*m*	Xxx
Mimochrome I	1	4	His
Mimochrome II	5	5	His
Mimochrome III	5	5	Ser
Mimochrome IV	1	4	His

Figure 1. Schematic representation, depicting the mimochrome chemical structures. The numbering scheme according to the IUPAC nomenclature is also reported; commonly, the position 5, 10, 15 and 20 have been also referred to as *meso*-positions.

In order to drive the folding of mimochromes into a unique diastereomeric form, or into stable, non interconvertible diastereomers, we refined the structure by design. Two strategies were used to reduce the peptide flexibility: i) by elongating the peptide chain at the C-termini, with a four residue fragment, modeled in an extended conformation; ii) by amino acid substitutions that may provide *intra*-molecular, *inter*-chain interactions.

The first strategy was successfully applied, as reported for mimochrome II, where the stabilization of the Δ isomer was achieved.[5d] The second strategy led to the design of mimochrome IV, namely 3,7,12,17-tetramethylporphyrin-2,18-di-N_8ε-(Ac-Glu^1-Ser^2-Gln^3-Leu^4-His^5-Ser^6-Asn^7-Lys^8-Arg^9-NH_2)-propionamide, described herein.

Results

Design: Mimochrome IV was designed by using the NMR structures of Co^{III}–mimochrome I Δ and Λ isomers as templates.[5b] Mimochrome I contains two leucine residues at both the N- and C-termini. These residues were selected in the initial design of mimochrome I, because of their high propensity to be accommodated in α-helical conformation.[3b] Further, we expected that hydrophobic interactions, between the leucine side chains and the porphyrin, would drive the helices to lay on the porphyrin. Nevertheless, as mentioned in the introduction, the sandwich was stable for the Co^{III} derivative, and not for the Fe^{III}.[5a,b] In order to provide an additional contribution to the stability of the sandwich, beside the metal coordination force, we modified the sequence of mimochrome I, by introducing *intra*-molecular *inter*-helical interactions. The Cα atoms of Leu^1 of one helix and of Leu^9 of the other helix are about 12 Å apart in both isomers (see Figure 2c). At this distance, the carboxylate side chain of a Glu residue at position 1 of one peptide chain could ion pair with the guanidine group of an Arg residue at position 9 of the other peptide chain (both side chains being modeled in an appropriate extended conformation). This condition may occur for both Λ and Δ isomers. It is expected that these substitutions may perturb the helical conformation marginally, because of the high propensity of Arg and Glu for helical structure.[3b,11] Actually, a positively charged residue (Arg) at the C-terminus, and a negatively charged residue (Glu) at the N-terminus reduces the intensity of the helix dipole and the helix would be more stable.[11] Thus, mimochrome IV differs from mimochrome I for Glu^1 and Arg^9, which replace Leu^1 and Leu^9, respectively. Further, the solvent exposed Ala^2 and Ala^6 in mimochrome I

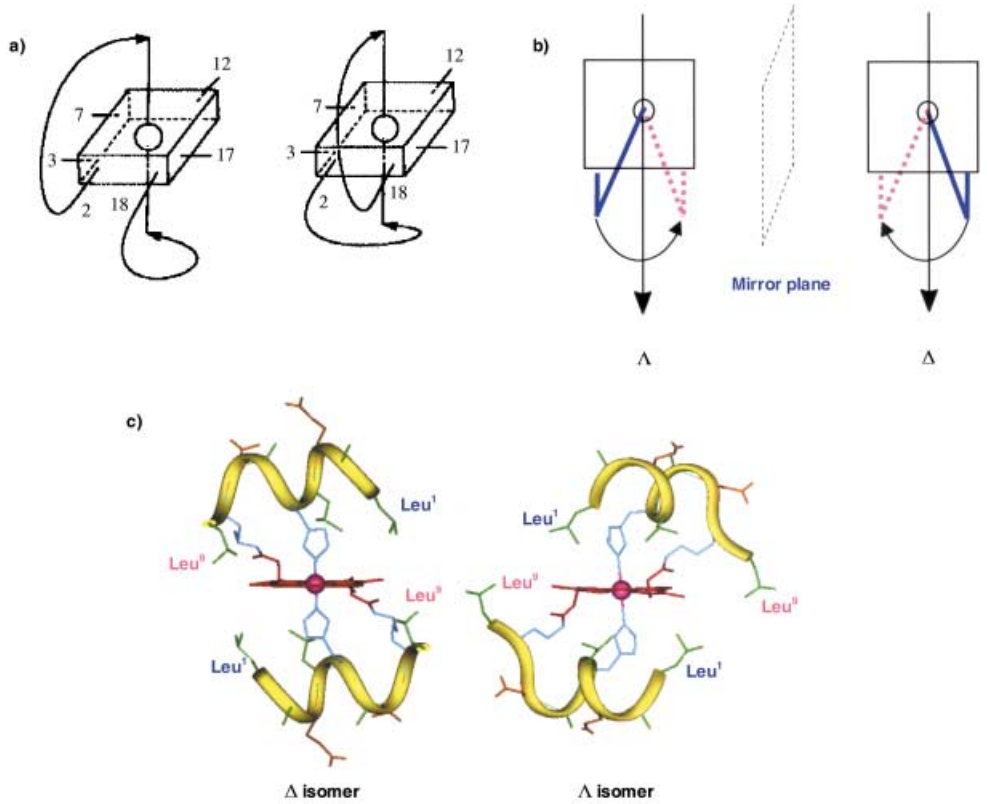

Figure 2. Mimochrome Λ and Δ isomers. a) Schematic representation depicting the different topologies adopted by mimochromes, upon His to metal ion coordination: each peptide chain can be arranged above or below the porphyrin plane, giving rise to diastereomeric configurations. b) Schematic diagram depicting how the absolute configuration is defined: two segments, connecting the Nε atoms and the positions 2 and 18 of the deuteroporphyrin ring, exemplify the peptide chains. In this presentation the molecule contains a C_2 axis as unique symmetry element and it must be chiral. The Δ isomer is defined as that obtained when, viewing along the Nε–M direction, the closest chain must be rotated clockwise to overlap the other chain. Due to the substituents on the porphyrin ring and to the chirality of the peptide chain, the Δ and Λ isomers are diastereomers. c) Average molecular structures of Co^{III}–mimochrome I Δ and Λ isomers, as obtained from NMR experimental data and RMD calculations.

were replaced by Ser residues in mimochrome IV, in order to further increase the water solubility of the new molecule.

Synthesis and RP-HPLC analysis: Mimochrome IV was synthesized by using the Fmoc chemistry and following the procedure previously developed;[5a] it was purified to homogeneity by RP-HPLC. MALDI-TOF mass spectrometry confirmed the expected molecular weight. The mimochrome IV Co^{III} and Fe^{III} complexes were successfully prepared by following the acetate method.[12] The RP-HPLC analysis of the reaction mixture for both Co^{III}- and Fe^{III}–mimochrome IV showed a single main peak. This may indicate that: i) a unique diastereomer is formed upon coordination of the histidines to the metal ion; or ii) the histidines are not axially ligated in the acidic HPLC conditions. This second hypothesis was excluded for the Co^{III} complex, by inspection of the UV/Vis spectrum (from the on-line diode array detector, 190–800 nm wavelength), which denoted bis-His axial ligation. Thus, the RP-HPLC analysis is the first experimental evidence of stabilization of one of the two possible isomers that may form upon coordination of the His residues to the cobalt center, even at acidic pH values. However, at this stage, it was not possible to assign the Δ or Λ stereochemistry to this new compound. For Fe^{III}–mimochrome IV, the two histidines are not axially ligated to the iron ion, at the acidic HPLC conditions, as detected by the on-line UV/Vis detector; as a consequence, no diastereomer may exist in these experimental conditions.

UV/Vis spectroscopy: UV/Vis spectroscopy was used to verify the metal insertion into the porphyrin ring, and to determine the coordination geometry, the spin and oxidation states of the metal ion. Figure 3 shows the UV/Vis spectra of Fe^{III}–mimochrome IV (Figure 3a) and Co^{III}–mimochrome IV (Figure 3b), in 0.3 mM phosphate buffer solution, pH 7.3. The observed spectral changes in both the Soret and visible regions, upon reaction of the free-deuteroporphyrin (Soret absorption maximum at 396 nm) with the metal ions, clearly denoted metal insertion into mimochrome IV. The position and the relative intensities of the Soret, β and α bands give useful information on the metal ion coordination state.[4b,12] For the iron derivative at pH 7, the positions of the Soret and low energy bands at 401 ($\varepsilon = 103\ mM^{-1}cm^{-1}$) and 522 nm ($\varepsilon = 6.18\ mM^{-1}cm^{-1}$), respectively, with a shoulder at ≈ 560 nm are indicative of a ferric low-spin state, with a bis-His axial coordination.[4b,12] For the cobalt complex at pH 7, the positions of the Soret, β and α bands at 415 nm ($\varepsilon = 163\ mM^{-1}cm^{-1}$), 525 nm ($\varepsilon = 11.8\ mM^{-1}cm^{-1}$) and 556 nm ($\varepsilon =$

8.24 $mM^{-1}cm^{-1}$), respectively, and the extinction coefficient ratio between the β and α bands are characteristic of an octahedral Co^{III}.[5b,d,13]

All the spectral data are very similar to those found for the Fe^{III} and Co^{III} complexes of mimochrome I and II.[5] Figure 3c shows selected UV/Vis spectra of Fe^{III}–mimochrome IV at different pH (from pH 2 to 7). Lowering the pH below 5 results in a blue shift of the Soret band absorption maximum from 401 to 388 nm. The spectral features at acidic pH (absorption maxima at 388, 494, 613 nm, for the Soret, β and α bands, respectively) are in agreement with a high spin state for the iron, axially coordinated by two weak ligands

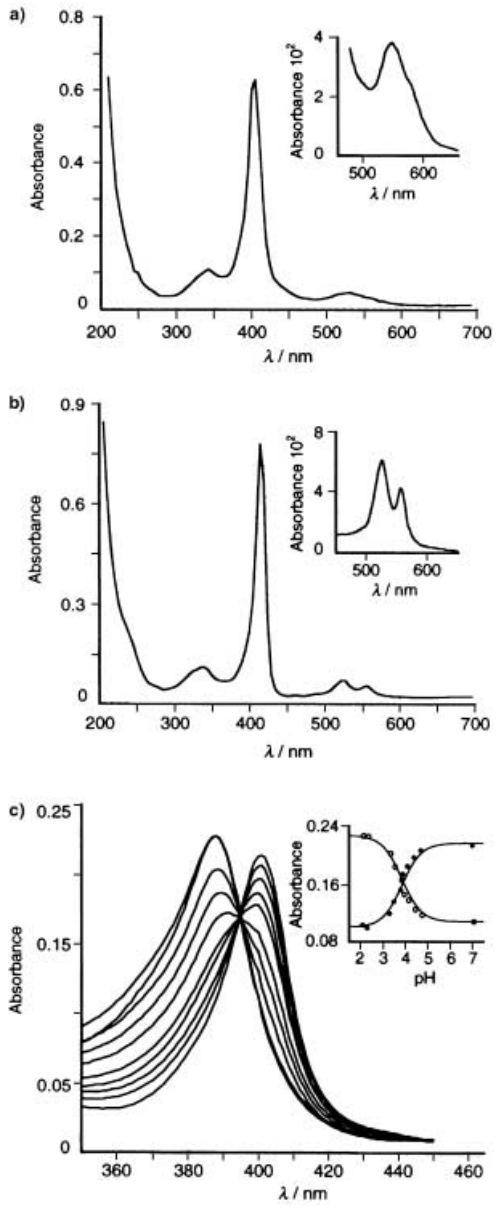

Figure 3. UV/Vis spectral properties of mimochrome IV. a) Fe^{III}–mimochrome IV 6.12×10^{-6} M in 0.30 mM phosphate buffer pH 7.3. b) Co^{III}–mimochrome IV 4.85×10^{-6} M in 0.30 mM phosphate buffer pH 7.3. Insets: expanded visible region. c) Soret region spectra of Fe^{III}–mimochrome IV at different pH values (pH 2–7). Inset: plot of the absorbance changes at 401 (●) and 388 nm (○) as a function of the pH.

(i.e., water molecules).[4b] By raising the pH above 5, the Soret band maximum shifts toward longer wavelength, thus indicating the formation of a strong ligand field on the iron porphyrin, typical of a bis-His coordination. The presence of an isosbestic point suggests that only these two species are predominantly involved in the equilibrium. Inset of Figure 3c reports the variation in the absorbance values at 401 and 388 nm, as a function of pH. Both titration curves exhibit a midpoint at pH 3.85 ± 0.14. Since the Fe^{III}–imidazole complexes are exchange-labile, the observed pH value accounts for the competition equilibrium between the coordination of the His axial ligand(s) to the heme iron and the protonation of the His in the uncoordinated form. Thus, the inflection point value represents the apparent pK_a for the protonation of the axially coordinated histidines (pK_{app}), as defined by Kennedy et al.[14] This means that at any given pH there is some population of His side chains not coordinated to Fe^{III} and available for protonation.

Circular dichroism spectroscopy: In order to analyze the peptide conformation and the mode of interaction of the peptide environment with the metalloporphyrin moiety, the CD spectra were recorded both in the far-UV and Soret regions. Figure 4 shows the CD spectra in the far-UV and Soret regions for the Fe^{III} (Figure 4a and b) and Co^{III} (Figure 4c and d) complexes, in 0.30 mM phosphate buffer, pH 7.0, at different TFE concentration. Table 1 reports the typical CD parameters, together with those of mimochrome I.

The CD spectral behaviors for both Co^{III}- and Fe^{III}–mimochrome IV complexes clearly indicate the peptides to be in helical conformation, as designed. The shapes and relative intensities of the minima around 222 and 207 nm, as well as the λ_0 crossover and maximum around 190 nm, indicate the peptides to be helical in both Fe^{III} and Co^{III} complexes, even in the absence of helix-inducing solvents (such as TFE).[15]

A comparison of Figure 4a and c shows that in aqueous buffer solution, the Fe^{III}–mimochrome IV complex is much helical, with respect to the Co^{III} species. The addition of TFE results in an increase of the helical content for both species just as expected. Complete helix formation was established at 30% TFE (see inset of Figure 4a and c); in this condition the peptides show similar helical content in both complexes.

The CD features of Fe^{III}- and Co^{III}–mimochrome IV were also investigated in the 400 nm region; Figure 4b and d display the CD spectra in the Soret region at different TFE concentrations, for the Fe^{III}- and Co^{III}-complex, respectively. Both complexes are characterized by the presence of a positive Cotton effect in the Soret region, with maxima at 398 and 414 nm for the iron and the cobalt complex, respectively. The intensity of the Cotton effect slightly increases upon TFE addition (up to 30%). A positive Cotton effect at 419 nm was observed for the Λ isomer of Co^{III}–mimochrome I.[5b]

Figure 4e reports the plot of the 398 nm band intensity as a function of the pH. The intensity of the Cotton effect decreases by lowering the pH, with a midpoint transition at pH 3.85. The same value was found for the pH induced ab-

Table 1. CD parameters of mimochrome IV and I metal derivatives.[a]

Species	UV Region $[\theta]_{min}\times10^{-3}$[b] ($\lambda$, nm)	$[\theta]_{222}\times10^{-3}$	$[\theta]_{ratio}$[b]	λ_0, nm	$[\theta]_{max}\times10^{-3}$ (λ, nm)	Soret Region $[\theta]\times10^{-3}$[b] (λ, nm)
Fe^{III}–mimochrome IV	−11.2 (207)	−9.54	0.85	200.1	16.8 (193)	31.8 (396)
Co^{III}–mimochrome IV	−15.2 (207)	−11.4	0.75	200.3	21.8 (192)	46.6 (413)
Fe^{III}–mimochrome I[c]	−11.3 (205)	−6.17	0.56	198.1	16.4 (190)	−22.0 (395)
Co^{III}–mimochrome I Λ[d]	−14.7 (204)	−6.50	0.44	197.7	22.2 (190)	27.1 (417)
Co^{III}–mimochrome I Δ[d]	−17.1 (204)	−8.70	0.51	197.3	25.1 (189)	−57.0 (416)

[a] Parameters are derived from the experimental CD spectra recorded under the conditions indicated in the Experimental Section, in 30% TFE/phosphate buffer (0.30 mM, pH 7.0). [b] $[\theta]$ are expressed as mean residue ellipticities (deg cm^2 dmol^{-1} res^{-1}) in the UV region, and as total molar ellipticities (deg cm^2 dmol^{-1}) in the Soret region; λ is expressed in nm; $[\theta]_{min}$ represents the ellipticity at the shorter wavelength minimum; $[\theta]_{ratio}$ represents the ratio of the ellipticity at 222 nm to that at the shorter wavelength minimum. [c] Data taken from ref. [5a]. [d] Data taken from ref. [5b].

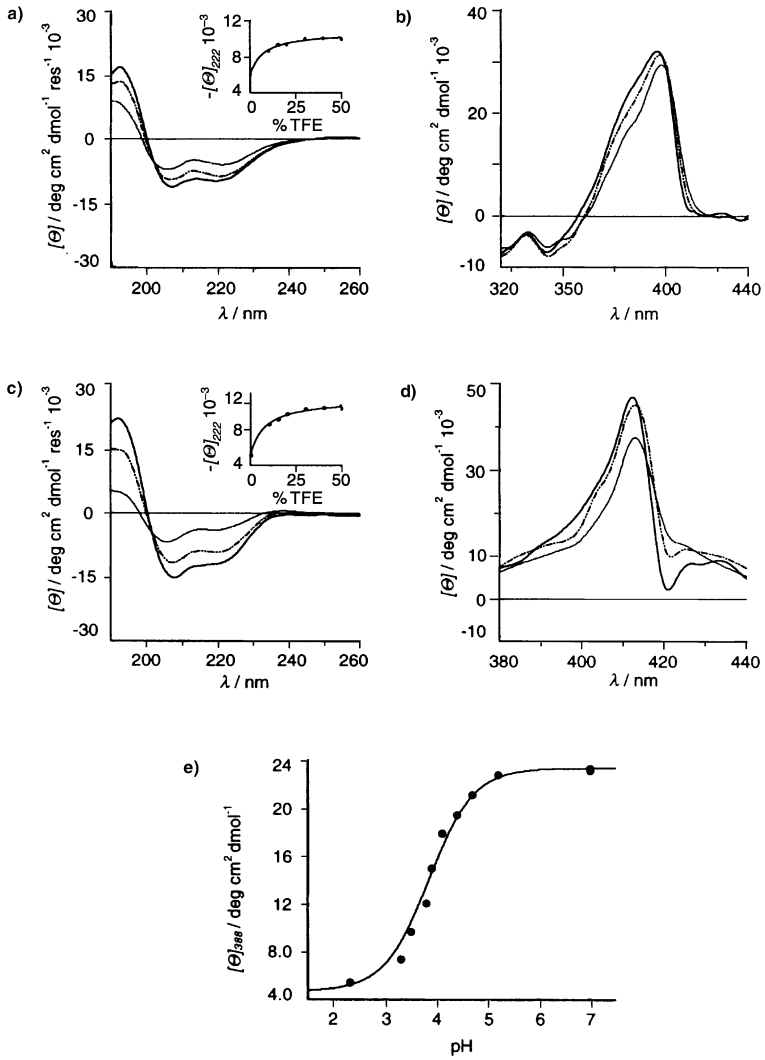

Figure 4. CD spectral properties of mimochrome IV. CD spectra of Fe^{III}–mimochrome IV in the a) far-UV region, and b) Soret region, and of Co^{III}–mimochrome IV in the c) far-UV region, and d) Soret region. Spectra were recorded at 6.41×10^{-6} M and 3.27×10^{-6} M concentration, for the Fe^{III}- and Co^{III}-derivative, respectively, in phosphate buffer (0.30 mM, pH 7.0)/TFE, at different ratios. e) Plot of the 398 nm band intensity, for Fe^{III}–mimochrome IV, as a function of the pH.

sorption transition in the Soret region (see Figure 3c), clearly indicating that they both refer to the same phenomenon.

NMR spectroscopy—Resonance assignment: The ^{1}H spectrum of Co^{III}–mimochrome IV shows a single set of resonances for the deuteroporphyrin protons and two set of resonances for the peptide chains. Homologous residues (belonging to different peptide chains) show distinct resonances for the backbone protons (αCH and NH), and severe overlaps for some side chain protons (see Supporting Information). Resonance assignments were accomplished by 2D experiments (NOESY,[16] TOCSY,[17] DQF-COSY,[18]) using standard methodologies[19] (see Supporting Information). However, it was not possible to distinguish the resonances of the peptide chain linked to the propionic group at position 2 from those of position 18 of the deuteroporphyrin ring (see Figure 1 for deuteroporphyrin numbering). The α,α′CH_2 protons of 2 and 18 propionic groups overlap at $\delta=$ 4.90 and 4.35 ppm, and the β,β′CH_2 protons overlap at $\delta=$ 3.35 and 2.95 ppm.

Structure from the NMR data: The structure determination of Co^{III}–mimochrome IV was based on the intensity of sequential and medium range NH–NH and αCH–NH NOE signals, on the magnitude of $^3J_{NH-\alpha CH}$ coupling constants, and on the characteristic non random-coil αCH chemical shifts (Figure 5).

250 NOEs were assigned and integrated, from the 2D NOESY map. 26 of the signals were NOE interactions between the peptide side chain and deuteroporphyrin protons. The relative intensities of the structurally considerable NOE cross-peaks are shown in Figure 5a.

Both peptide chains showed a very similar pattern of NOE interactions, which strongly support the presence of a well-organized structure. A right-handed helical conformation could be inferred from Glu^1 to Asn^7 on the basis of charac-

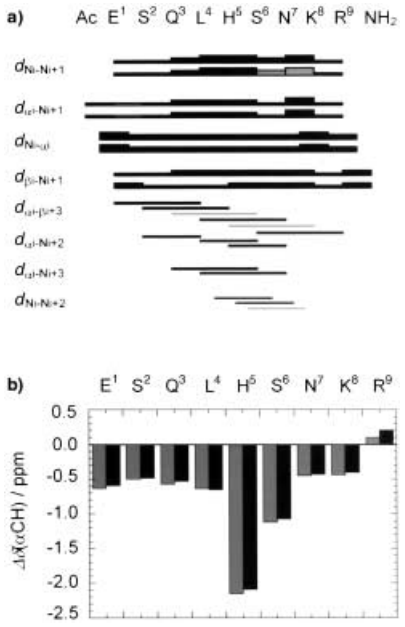

Figure 5. Ability of mimocrome IV to fold up into a helical structure. a) Summary of the NOE connectivities. Solid lines indicate unambiguous NOEs. Line thickness reflects the intensity of the NOE connectivities. b) Chemical shift index $\Delta\delta(\alpha CH)$. All protons show distinct resonances for the two peptide chain.

teristic short-range NH–$NH_{(i,i+1)}$, αCH–$NH_{(i,i+1)}$, βCH–$NH_{(i,i+1)}$, and medium-range αCH–$\beta CH_{(i,i+3)}$, NH-$NH_{(i,i+2)}$, αCH–$NH_{(i,i+3)}$ NOE signals.[19] A non-regular structure occurs at the C-terminal end, which displays only few of the connectivities expected for a helical conformation. The $^3J_{NH-\alpha CH}$ coupling constant values confirmed these findings (see Supporting Information). The αCH chemical shifts were additional indicators of helical structure (Figure 5b).

All residues, and particularly His^5, showed αCH chemical shifts significantly up-field shifted, relative to their random coil values.[20] Since this trend was observed also for the C-terminal residues, it is reasonable to assume that these deviations are due not only to peptide secondary structure but also to the deuteroporphyrin ring current effect.[21]

NOE contacts between the His^5-εCH and Glu^1 side chain protons were observed for both peptide chains; they were unambiguous, since the His^5 imidazole protons resonate in the high field region of the spectrum and give distinct resonances for each peptide chain. These contacts allowed us to correctly orient the imidazole with respect to the peptide backbone. The Co^{III} axial ligation occurs through the unprotonated imidazole Nε atom of the histidines, as in the Co^{III}–mimochrome I complex.[5b] Further, the δCH and εCH imidazole protons have different connectivities with the deuteroporphyrin protons. These connectivities were crucial to define the orientation of the His^5 imidazole rings with respect to the deuteroporphyrin ring. One histidine exhibits εCH ↔ 10H, εCH ↔ $12CH_3$, εCH ↔ 15H, εCH ↔ 13H, δCH ↔ $3CH_3$ and δCH ↔ 5H dipolar contacts; the other histidine exhibits εCH ↔ 5H, εCH ↔ 8H, εCH ↔ 10H and δCH ↔ 15H, δCH ↔ $17CH_3$, δCH ↔ 20H NOE dipolar contacts. One imidazole ring presumably lies in a plane that is orthogonal to the deuteroporphyrin plane and that intersects the deuteroporphyrin plane close to the 1 and 11 positions, while the other imidazole plane intersects the deuteroporphyrin plane close to the 6 and 16 positions (Figure 6a).

The observed NOE contacts between peptide side chains (Leu^4, His^5, Lys^8 and Arg^9) and deuteroporphyrin protons, together with simple stereochemical considerations, allowed us to correctly position the two peptide chains with respect to the deuteroporphyrin ring. Figure 6b depicts qualitatively the final interpretation. Chain 2a was named the one bound to the propionyl group at position 2, and chain 18b the one bound to the propionyl group at position 18. Furthermore, due to the right-handedness of the α-helices, chain 2a must lie above the plane of the deuteroporphyrin and chain 2b is positioned below this plane, when the porphyrin is seen as in Figure 7.

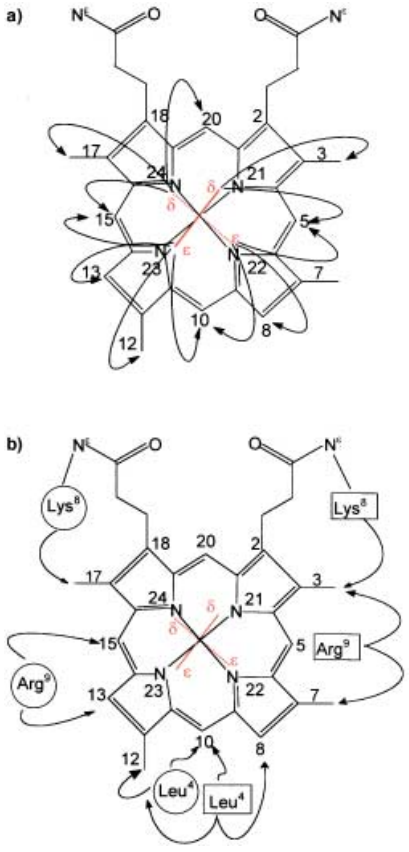

Figure 6. Positioning the imidazole histidines and the peptide chains, with respect to the porphyrin ring in Co^{III}–mimochrome IV. a) Schematic presentation of the NOE connectivities (arrows) between His^5-εCH (ε) and δCH (δ) protons and the deuteroporphyrin protons. When viewing along the axial bond direction, the imidazole rings appear as segments, which are reported as red continuous or dashed lines (above or below the deuteroporphyrin ring, respectively). b) Schematic presentation of the NOE connectivities (arrows) between Leu^4, Lys^8 and Arg^9 side chain protons and the deuteroporphyrin protons. Residues belonging to the peptide chain 2a are inserted in a circle, and residues belonging to the peptide chain 18b are inserted in a square. The coordinated imidazole rings are represented as a red continuous or dashed line.

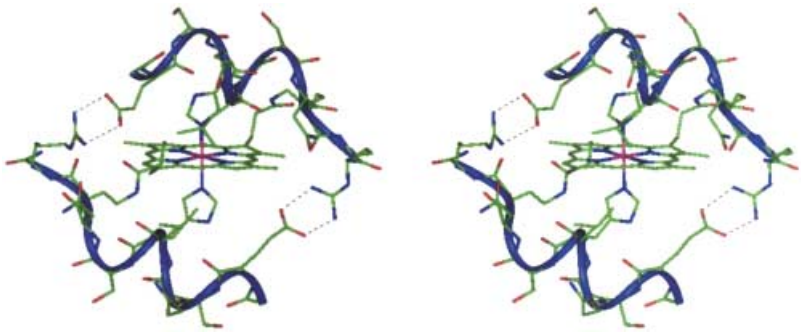

Figure 7. Molecular structure of Co^{III}–mimochrome IV. Stereo view of the average structure, as obtained from NMR experimental data and RMD calculations.

Molecular dynamic calculations: All the information described in the previous paragraph allowed us to build a reasonable initial model for Co^{III}–mimochrome IV. This model was refined by RMD calculations in vacuo at 300 K. Table 2 reports the average backbone molecular conformation, along the trajectory of the RMD. In the final model (see Figure 7), the two peptide chains adopt quite similar conformations. The chain 2a assumes ϕ and ψ angles very close to those expected for a right-handed α-helical conformation, except for the Lys^8 and Arg^9 C-terminal residues. The chain 18b adopts a less regular conformation, since also the residues Leu^4 and Asn^7 slightly deviate from a regular α-helical conformation. The mean values of the ϕ and ψ angles, calculated for the residues Glu^1–Asn^7, are -59 ± 17; -41 ± 17, for the chain 2a, and -64 ± 30; -31 ± 14, for the chain 18b.

Table 2. Average torsion angles [°] of Co^{III}–mimochrome IV as obtained from RMD simulation.

	Chain 2a[a]			Chain 18b[a]		
Residue	ϕ	ψ	χ^1	ϕ	ψ	χ^1
Glu^1	−59	−28	−81	−59	−38	−87
Ser^2	−26	−65	74	−26	−54	−52
Gln^3	−56	−43	−172	−59	−21	−167
Leu^4	−65	−47	−71	−106	−38	−73
His^5	−78	−11	−56	−57	−30	−66
Ser^6	−74	−43	−52	−39	−24	−170
Asn^7	−54	−51	179	−100	−7	−170
Lys^8	62	−69	−179	13	−49	−170
Arg^9	−124	40	−58	58	−57	−55

[a] Chain 2a and 18b refer to the peptide chain linked to the propionyl group at position 2 and 18 of the deuteroporphyrin ring, respectively.

For both peptide chains, all peptide bonds are *trans* and all side chain conformations are staggered. A $C'O_i \leftarrow HN_{i+4}$ almost regular pattern of intra-chain hydrogen bonds was found for the peptide chain 2a (see Supporting information), except for the lack of His^5-$C'O \leftarrow Arg^9$-NH hydrogen bond and for the presence of two $C'O_i \leftarrow HN_{i+3}$ hydrogen bonds at the N-terminal. A less regular pattern of intra-chain hydrogen bonds was observed in the peptide chain 18b. The local conformational arrangements observed in the chain 18b, produce an increase of the distances between the C′O group of Leu^4 and the NH of Lys^8, and between the C′O group of Gln^3 and the NH of Asn^7, resulting in the breaking of the corresponding hydrogen bonds. As a consequence, only two $C'O_i \leftarrow HN_{i+4}$ hydrogen bonds ($C'O_1 \leftarrow HN_5$ and $C'O_2 \leftarrow HN_6$) are present; all the other residues are involved in $C'O_i \leftarrow HN_{i+3}$ hydrogen bonds. In addition, the NH of Lys^8 and the NHε of Arg^9 form hydrogen bonds with the C′O groups of His^5 and Asn^7, respectively.

The helix axes were found to be about parallel to the deuteroporphyrin plane and to form an angle of about 80° with each other, in good agreement with the designed model.

The Leu^4, His^5 and Lys^8 side chains are facing the deuteroporphyrin plane while the side chains of hydrophilic residues (Ser^2, Gln^3, Ser^6 and Asn^7) are exposed to the solvent. The Glu^1 and Arg^9 side chains, of both peptide chains, face each other, and as a consequence the guanidine group of Arg^9 belonging to the one peptide chain forms an ion pair with the carboxylate side chain of Glu^1 of the other peptide chain, and vice versa.

Redox potential determination: The Fe^{III}/Fe^{II} reduction potential (E) was determined by direct current (DC) cyclic voltammetry at a pyrolytic graphite (PG) electrode, containing on the surface a microlayer of tributylmethyl phosphonium chloride (TBMPC) membrane entrapping mimochrome IV (see the Experimental Section for details).[22] Figure 8 shows the cyclic voltammograms at pH 3.0, 7.0 and 9.2.

Figure 8d also shows the pH dependence of the redox potential for iron–mimochrome IV. Three different regions are clearly evident: two regions (pH ranges 2–4 and pH 7–10), where the major dependence of E on pH occurs; and one region (pH range 4–7) where the E value is quite independent on pH. The data can be fit according to the [Eq. (1)] in the Experimental Section, which account for the presence of (at least) two acid/base groups, whose protonation affects the heme redox potential. Analysis of the data gave the pK_a values of the two groups ($^{ox}pK_{a1}=3.86\pm0.12$, $^{red}pK_{a1}=2.99\pm0.11$; $^{ox}pK_{a2}=8.46\pm0.11$, $^{red}pK_{a2}=7.79\pm0.12$) in the oxidized and reduced forms of the heme.

Discussion

Several strategies were conceived to obtain metalloprotein models.[2–4] For heme-protein models, the use of two parts that associate around the heme, to give folded covalent or non-covalent self-assembled dimers was particularly success-

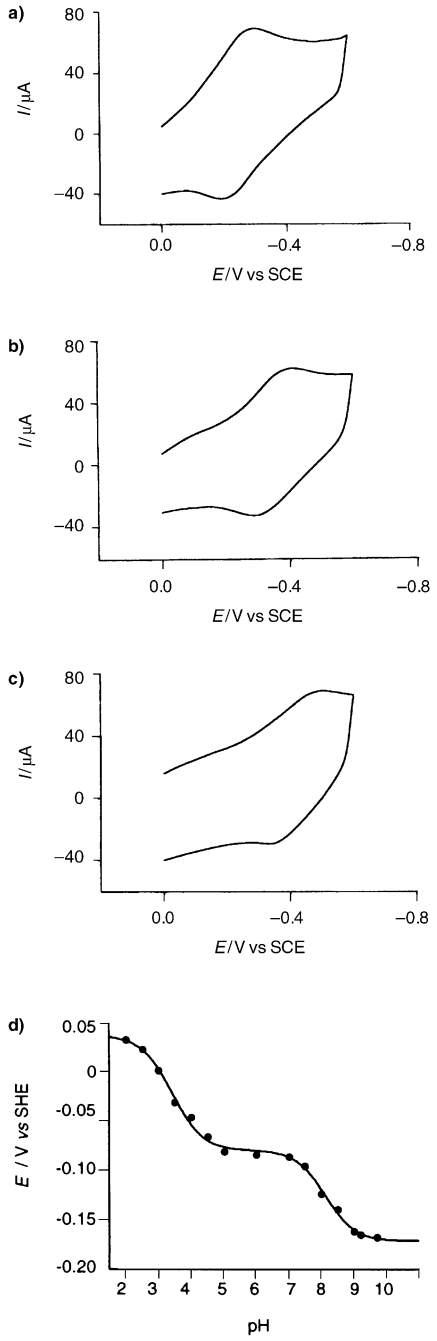

Figure 8. pH dependency of the redox potential E for Fe^{III}–mimochrome IV complex. Cyclic voltammograms (25 °C, scan rate 1.0 $V s^{-1}$), over a potential range between 0.2 and −0.8 V against SCE, at pH 3.0 (a), 7.0 (b) and 9.2 (c). E vs pH data set (d). The fitting of the curve to equation 1 yielded the following values: $^{ox}pK_{a1} = 3.86 \pm 0.12$; $^{red}pK_{a1} = 2.99 \pm 0.11$, $^{ox}pK_{a2} = 8.46 \pm 0.11$; $^{red}pK_{a2} = 7.79 \pm 0.12$.

ful (for recent reviews see ref. [3e,4]). Numerous models are homo-dimers with C_2 symmetry related components. The use of the symmetry is quite advantageous, on one hand, because it simplifies the design, the synthesis and the structural characterization, but, on the other hand it may lead to diastereomeric forms.[6b] This problem was encountered in the study of mimochromes.[5a–c] In fact, stable Λ and Δ isomers of Co^{III}–mimochrome I were unpredicted, but experimentally observed.[5b] The rapid kinetics of interconversion between the two diastereomeric forms in Fe^{III}–mimochrome I caused a poor solubility in water, thus limiting its possible application as a functional heme–protein mimetic. In this paper we propose a strategy to solve this problem: we modified the structure of mimochrome I, and inserted interactions between the two symmetric halves with the aim of 1) stabilizing only one of the two possible diastereomeric forms, or limiting the exchange between multiple species; 2) increasing the water solubility. As outlined above, the insertion of Glu and Arg residues at position 1 and 9 of the sequence, respectively, was successful in stabilizing the sandwich structure and in favoring the formation of one isomer over the other, both in the Fe^{III} and Co^{III} complexes. This may lead to the observed increased solubility of mimochrome IV in aqueous solution (up to mM concentration), either as free-base form, or as iron and cobalt complexes. It remains to be ascertained why only one isomer is favored. Modeling suggested that the same hydrogen-bond and ion-pair interactions occur in both Δ and Λ diastereomers. In contrast, interactions between the asymmetric sides of the deuteroporphyrin (methyls 3 and 7 on one side, and methyl 17 on the opposite side) and the side chains of Arg[9] are more favorable in the Λ isomer, than in the Δ. These hydrophobic interactions may account for the unfavorable loss in entropy, which occurs when one isomer is stabilized over the other.[3b] The lack of these hydrophobic interactions in mimochrome I may also account for the different behavior of its Co^{III} complex respect to mimochrome IV.

Both iron and cobalt complexes were characterized by UV/Vis spectroscopy. A good agreement with the spectral features previously observed for mimochrome I and II was found. The UV/Vis spectra of both Fe^{III}- and Co^{III}–mimochrome IV, at pH 7, are typical of octahedral bis-His low spin complexes (Figure 3), as expected. For the Co^{III} complex, the bis-His coordination occurs even at very acidic conditions (pH < 2). This finding is related to the high preference of cobalt for nitrogen donor ligands, and to the exchange-inertness of low-spin Co^{III} complexes. In the low spin hexa-coordinated iron(III) complex, which is exchange-labile, a coordination pH-dependent behavior can be observed. Both the imidazoles of the axially coordinating His display an Nε $pK_{app} = 3.85 \pm 0.14$, indicating that the bis-His coordination represents over 90% of the population at pH > 4.85 (Figure 3c). The strength of the axial bonds increases upon reduction of the iron atom, as suggested by the lower pK_{app} value (2.99 ± 0.11) observed in the iron(II) form (Figure 8d). The low pK_a values of the axially coordinating His (with values very close to what observed in several myoglobins, hemoglobins and cytochromes in the oxidized and reduced forms) strongly support the designed sandwich structure.[23] The hydrophobic interactions between the Leu[4] and Lys[8] side chains and the deuterohemin ring drives the imidazole–metal coordination, with the consequent formation of the sandwich. In this structure, the two His side chains result buried in a high hydrophobic environment, which lowers the pK_a values. It is also worth mentioning that the different imidazole His pK_a values, found for Fe^{III} complexes of mimochrome I and IV (2.5 and 3.85, respectively), may be attributed to the substitution of the hydro-

phobic Leu at positions 1 and 9, with Glu and Arg, respectively. The more polar environment around the His residues, in mimochrome IV, may cause an increasing in the pK_{app} value of about one pH unit, either by changing the equilibrium constant for Fe^{III}–His coordination, by altering the pK_a of the dissociated His ligand, or both.

CD measurements in both the UV and Soret regions gave preliminary structural information on mimochrome IV. Analysis of the UV region indicates the peptides to be in helical conformation, in both iron and cobalt complexes. The helical content increases upon TFE addition (up to 30%) (Figure 4), and it is higher than that of the corresponding mimochrome I complexes. This finding clearly indicates that the amino acid substitutions made in the mimochrome I sequence did not perturb the helical conformation of the peptide chains, but they play a favorable contribution in the helix formation. The θ_{222} values for both Co^{III} and Fe^{III} complexes are lower than that expected for an almost complete helical conformation. Indeed, the NMR results (see the following) indicate that the two peptide chains in Co^{III}–mimochrome IV are in a quite regular α-helical conformation (≈80% of the residues). Even though the θ_{222} value can be correctly applied to calculate the helix percentage in proteins, it fails to estimate the helix contents in small peptides,[24] for which the θ ratio of the minimum at 222 nm to the minimum at shorter wavelengths, the position of this last minimum and the crossover wavelength λ_0 are all indicative of helix propensity. Further, the interactions between the heme transitions and those of the peptide backbone amide dipoles may influence the far-UV CD spectra.[7a,25] This is obviously much evident in small peptide–porphyrin systems, respect to heme proteins. All these findings may explain the apparent disagreement between CD and NMR data. Fe^{III}–mimochrome IV is more helical than the corresponding cobalt complex in the absence of the helix-inducing solvent TFE. This behavior may be tentatively attributed to a different binding affinity of the two histidine ligands for Fe^{III} and Co^{III}. Stronger coordination strength in the Co^{III} complex may induce a significant geometric restriction on the coordinating His residues, with consequent distortion of the two helices. The TFE addition, through the induction of a more helical conformation in both complexes, smoothes the differences observed at 0% TFE.

The examination of the CD spectra in the Soret region is very interesting, in order to correlate the sign of the Cotton effect with the configuration around the metal ion, that is, Δ or Λ. Both iron and cobalt complexes exhibit positive Cotton effects, whose intensity slightly increases with increasing TFE concentration (Figure 4). This finding, already observed for mimochrome I and II,[5] proves that the intensity of the Cotton effect is strictly related to the helical content of the peptide chains. Further, it confirms our previous hypothesis that the origin of the induced Soret Cotton effect in such molecules can be ascribed to the coupling between porphyrin (π–π*) and peptide backbone (n–π* and π–π*) transitions. Further evidence came from the pH titration: the intensity of the Soret Cotton effect decreases by lowering the pH value, and the ellipticity at 398 nm essentially disappears at pH <2 (Figure 5e). The mid-point value was observed at pH 3.85. The same value was also derived from the UV/Vis pH titration (see Figure 3c), and it was attributed to the apparent pK_a value of the two coordinating histidine residues. This finding could indicate that a similar phenomenon accounts for the pH dependence of the spectral behaviors and of the Soret Cotton effect. Lowering the pH increases the percentage of His side chain that are protonated, rather than coordinated to the iron. As a consequence, the peptide chains move apart from the porphyrin plane, and the Cotton effect in the Soret region disappears.

We also observed that the sign of the Cotton effect depends on the relative orientation of the peptide chains respect to the porphyrin plane. In the cobalt complexes of mimochrome I and II, the Λ configuration gives rise to a positive Cotton effect, whereas the Δ configuration gives rise to a negative effect; in the Fe^{III}–mimochrome I complex, the observed S-shaped Soret Cotton effect was attributed to the simultaneous presence of the two diastereomeric forms. Consequently, the presence of a positive Cotton effect in both Fe^{III}- and Co^{III}–mimochrome IV complexes indicates that both systems assume a Λ configuration. A single positive Cotton effect detected even in the iron complex confirmed the effectiveness of the *inter*-helical interactions in reinforcing the sandwich structure and in driving the peptide chains to fold into a unique topology around the heme.

The definitive answer of the structural identity of the diastereomer stabilized in mimochrome IV was obtained by NMR structural characterization of the cobalt complex. The NMR analysis fully confirms the UV/Vis and CD data, both regarding the helical conformation of the peptide chains, and the Λ configuration of the hexacoordinated Co^{III} ion. The RMD calculations, using the NMR experimental data as conformational restraints, indicated two helical peptide chains, oriented about perpendicularly. The helix 2a adopts an almost regular α-helical conformation, whereas a squeezed helical winding toward a 3_{10}-helical arrangement characterizes the helix 18b. This finding is supported by the different pattern of *intra*-chain hydrogen bonds (see Table S2 in the Supporting information) and by the different mean values of the ϕ and ψ torsion angles. In more details, the helix 2a contains two complete α-helical turns; a partial distortion toward a 3_{10}-helical arrangement involves the residues Glu^1 and Ser^2; a γ-turn around Lys^8 is present at the C-terminus. A larger 3_{10}-helical content is observed for helix 18b; only the central residues open up toward α-helix, in order to better satisfy the geometric parameters required by the His^5 coordination. The differences in the local conformation observed for the two peptide chains can be justified by simple stereochemical considerations. The Glu^1, Leu^4, Lys^8 and Arg^9 side chains of each helix are facing different substituents of the deuteroporphyrin ring (see Figure 6b). As a result, the peptide backbones adjust their conformation in such a way to minimize steric repulsions between the peptide side chains and the deuteroporphyrin methyl groups.

A bis-axial coordination through the His^5-Nε atoms was determined. Both His^5-δNH groups are hydrogen bonded to the backbone oxygen atom of Glu^1, as found in several heme proteins.[26] The orientation of both imidazole rings was accurately determined on the basis of the NOE signals

between the deuteroporphyrin protons and the imidazole rings. The two imidazole planes adopt a perpendicular relative orientation, with each imidazole plane nearly eclipsing a N_p-Co-N_p bond (see Figure 6). Such perpendicular orientation of the axial ligand planes was found in several Co^{III}–porphyrin model compounds.[27] Finally, as already reported for Co^{III}–mimochrome I,[5b] the solution structure allowed us to ascertain the Λ configuration around the Co^{III} ion. The designed sandwich structure is further stabilized by interchains ion pairs between Glu^1 and Arg^9, and by hydrophobic interactions between Leu^4 and Lys^8 side chains and deuteroporphyrin. Similarly to the Λ isomer of Co^{III}–mimochrome I, Leu^4 and Lys^8 side chains create a partially open hydrophobic cage around the imidazole ring. Position 20 of the deuteroporphyrin ring is exposed to the solvent, while all the other *meso* positions are covered by the polypeptide chains. Serines, glutamines and asparagines are pointing outward from the molecular core, as designed.

The redox potential determination was carried out in order to determine the influence of the peptide chain on the iron–porphyrin properties. The heme redox potential in mimochrome IV is −80 mV (versus SHE) at pH 7, and it is modulated by the pH. In particular it is clearly pH dependent in two regions (Figure 8). The possible groups available for proton coupling to heme redox behavior are: 1) the coordinating His^5 residues; 2) the Glu^1 and Arg^9 residues.

In the low-pH region (pH range 2–4), the proton-linked change of the redox potential can certainly be attributed to the protonation of the His^5-Nε and dissociation of the axial ligands. The apparent $^{ox}pK_{a1}$ value (3.86 ± 0.12), calculated by fitting the redox titration curve according to Equation (1), agree well with that determined by UV/vis and CD spectroscopic titrations (3.85 ± 0.14; see Figures 3c and 4e) and unambiguously attributed to the axially coordinating His. All the titration data also indicate that the cleavage of the two axial histidines occurs at the same pH and independently from each other. In addition, in this region the protonation of the glutamate side chains would likely occur. Involvement of glutamate residues in redox-linked proton exchange was reported by Dutton and co-workers for heme–protein maquettes, and it was also suggested for natural cytochromes b and cytochrome c oxidase.[10b] The pK_a value of glutamate (4.25 when free in solution) is quite similar to that observed for the His^5-Nε in mimochrome IV, and therefore it is not possible to discriminate whether in the low-pH region the redox potential is affected by the protonation of one or two acid/base groups.

In the high-pH region (pH range 7–10), the pK_a value (i.e., $^{ox}pK_{a2} = 8.46 \pm 0.11$ and $^{red}pK_{a2} = 7.79 \pm 0.12$) for the redox-linked proton binding might be ascribed to the non-ligating His^5-Nδ. However, it must be outlined that deprotonation of the imidazole/histidine axial ligands is usually associated to a 5–7 nm red shift in the Soret absorption band.[10b] The absence of such a shift for Fe^{III}–mimochrome IV in the pH range 5–10 indicates that no deprotonation on the His^5-Nδ occurs over the pH range explored. Further, a change in the coordination geometry with the formation of a μ-oxo dimer [Fe^{III}-O-Fe^{III}] or a hydroxide complex [His-Fe^{III}-OH] should also be excluded,[28] because no changes in the UV/Vis spectrum are observed up to pH 9.5 (see Figure S2 in the Supporting Information). Therefore, an additional residue should be responsible for the observed redox-linked proton binding in this pH range. Analysis of the mimochrome IV structure left the Arg^9 residues as the only possible candidates to account for the *E*/pH relationship observed in the high-pH region. However, a decrease of four orders of magnitude in the Arg pK_a value, with respect to the normal value, is quite surprising and this hypothesis need further investigations to be completely proven.

It is finally to outline that iron–mimochrome IV shows a pH-independent redox behavior over a quite large range (4.5–7.5), around the physiological pH value.

In summary, mimochrome IV is a simple, structurally defined heme–protein model, which may provide an excellent opportunity for exploring the subtle mechanisms that control the heme functions. The peptide structure of mimochrome IV is such that a partially open hydrophobic cage around the imidazole ring is present. Except for the position 20 of the deuteroporphyrin ring, all the other *meso* positions are covered by the polypeptide chains, which, similarly to the natural systems, may protect the deuteroporphyrin ring from degradation during catalytic cycles.

The amino acid composition of mimochrome IV can be modified in order to modulate the functionality in terms of redox potentials, trying to adapt the behavior to different applications. Substitution of serines, glutamines and asparagines, which point outward from the molecular core, with differently charged residues may alter the electrostatics, polarity and solvent accessibility of the heme site, and modulate its electronic, catalytic and binding properties.

Experimental Section

Synthetic procedure: The synthesis of mimochrome IV was achieved on a Milligen 9050 automatic peptide synthesizer, as previously reported.[5a] It was purified by preparative reverse-phase HPLC, (Shimadzu instrument) on a Kromasil C_{18} column. The purified compound was analyzed by MALDI mass spectrometry (MALDI/MS) using a Voyager DE instrument (Perkin–Elmer), operating at the Centro di Metodologie Chimico-Fisiche, University Federico II of Napoli (M.W. 2753 amu).

Cobalt and iron were inserted into mimochrome IV according to the literature procedure.[12] The acetate of the metal (in the oxidation state II) (0.003 g, 1.3×10^{-5} mol) was added to a solution of pure mimochrome IV (0.010 g, 2.6×10^{-6} mol) in acetic acid/TFE (6:4, 6 mL). The reaction mixture was heated under reflux for 2 h at 45 °C. The reaction was monitored by analytical HPLC, and the desired product was purified to homogeneity by preparative HPLC. MALDI/MS confirmed the expected molecular weight (Co^{III}–mimochrome IV = 2810 amu; Fe^{III}–mimochrome IV = 2806 amu).

Analytical methods: Total metal-reconstituted mimochrome IV concentrations were determined on the basis of the metal content, derived from flame atomic absorption spectrometry. Standard procedures, on a Varian SpectrAA 220 atomic absorption spectrometer, equipped with a MK7 burner, were used.[29] Solutions containing approximately 50 mg L^{-1} of metal-reconstituted mimochrome IV (≈1 mg L^{-1} of metal; $\approx 2 \cdot 10^{-5}$ M) in ultra pure metal-free water were directly aspired into an air-acetylene flame with no prior treatment. Concentrations were obtained both by comparison with calibration curve and by standard addition. No differences, which overcome experimental uncertainty, were observed.

Stock grade 1000 ppm metal solutions, certified for metal and impurities content, were from ROMIL Ltd, Cambridge and from Inorganic Ven-

tures Inc., Lakewood. Working standards for iron and cobalt analysis were prepared daily by appropriate dilution of the stock solution with 3.6% hydrochloric acid and 2% nitric acid, respectively. Alternative working standards were also prepared by appropriate dilution of the stock solution with the same matrix of the samples. No differences in the absorbance values were observed over the experimental error.

Co^{III}- and Fe^{III}–mimochrome IV stock solutions, analyzed for metal contents, were appropriately diluted and used for determining the extinction coefficients at the Soret band maximum wavelength.

UV/Vis spectroscopy: UV/Vis spectra were recorded on a Perkin–Elmer Lambda 7 UV Spectrophotometer with 1 cm path length cells. Wavelength scans were performed at 25°C from 200 to 700 nm, with a 60 nm min^{-1} scan speed. Co^{III}- and Fe^{III}–mimochrome IV extinction coefficients at the Soret band maximum wavelength were determined in phosphate buffered solutions (pH 7; final phosphate concentration 3.0×10^{-4} M), using a concentrations range 1.0×10^{-6}–1.0×10^{-5} M.

Circular dichroism spectroscopy: CD spectra were obtained at 25°C on a Jasco J-715 dichrograph. Data were collected at 0.2 nm intervals with a 5 nm min^{-1} scan speed, a 2 nm bandwidth and a 16 s response, from 260 to 190 nm in the far-UV region. The spectra in the Soret region were collected from 470 to 360 nm for the cobalt complex, and from 500 to 300 nm for the iron complex. Cuvette path length of 1 cm was used for all spectral regions. Sample solutions at different TFE/aqueous phosphate ratio (from 0 to 50% TFE) were prepared for both Co^{III}–mimochrome IV (6.41×10^{-6} M) and Fe^{III}–mimochrome IV (3.27×10^{-6} M). CD intensities in the far UV region are expressed as mean residue ellipticities (deg cm^2 dmol^{-1} res^{-1}); intensities in the Soret region are reported as total molar ellipticities (deg cm^2 dmol^{-1}).

NMR spectroscopy: Proton NMR spectra were collected at 298 K on a Bruker Avance 600 MHz spectrometer (at the CERM, University of Florence), equipped with triple-resonance 5 mm probe. Co^{III}–mimochrome IV was used as a 1.0×10^{-3} M solution in H_2O/CF_3CD_2OD (70:30 *v/v*, pH 5.5). 2D NOESY,[16] TOCSY,[17] and DQF-COSY[18] were acquired using standard pulse sequences, on a spectral width of 7.6 kHz, collecting 4 K data points in F2, and 512 points in F1. Quadrature detection in F1 was achieved by using TPPI,[30] and the water resonance was suppressed by presaturation. Mixing times were 70 ms for TOCSY and in the range 120–350 ms for the NOESY spectra. Semi-quantitative information on interproton distance for structure calculation was obtained from the 200 ms NOESY spectrum that did not exhibit spin diffusion effects. The programs NMRPipe[31] and XEASY[32] were used for data processing and spectral analysis, respectively. The chemical shifts are relative to the sodium salt of [D_4]3-(trimethylsilyl)propionic-2,2,3,3-acid.

Computational details: All the computations were performed on a Silicon Graphic Octane2 workstation. The program package InsightII/Discover with the Extensible Systematic Force Field (ESFF),[33] was used for energy minimization and restrained molecular dynamic (RMD) simulation. The solution structure of the Co^{III}–mimochrome I Δ and Λ isomers,[5b] derived from the NMR analysis, was used as template for modeling the mimochrome IV molecule.

The initial model was examined for inconsistencies with the experimental NMR data (interproton distances from NOE values and $^3J_{NH-\alpha CH}$ coupling constants), and then subjected to RMD calculations, in vacuo at 300 K. The distance restraints in the RMD simulations were classified according to the relative intensity of the NOEs into four classes: 1.8–2.6 (strong), 2.5–3.3 (medium), 3.2–4.1 (weak) and 3.2–5.0 Å (very weak). A distance dependent dielectric constant was used through all computations. The equations of motion were solved using the Leapfrog integration algorithm, with a time step of 1 fs. The simulation protocol consisted of an equilibration period of 50 ps and of a simulation period of 400 ps. A structure was saved every 100 fs during the simulation for analysis. The final average structure was checked for consistency with all observable NOE.

Cyclic voltammetry: DC cyclic voltammetry was carried out at 25°C, employing a modified PG electrode (3 mm diameter).[22] Fe^{III}–Mimochrome IV was immobilized on a TBMPC membrane, which was dried out at 5°C on the electrode surface. Voltammograms were run between +200 mV and −600 mV vs a standard calomel electrode (SCE), at a scanning speed varying between 50 mV s^{-1} and 1000 mV s^{-1}. Experiments were performed employing as buffers 0.05 M acetate (pH < 5.5), 0.05 M phosphate (pH range 5.5 −8.0), carbonate (pH > 9.0). Under all conditions $KClO_4$ (up to a 0.1 M final concentration) was added in solution as a support electrolyte.

The pH dependence of the redox potentials for Fe^{III}–mimochrome IV was analyzed according to Equation (1):

$$E = E_0 \cdot ({}^{ox}K_{a1}[H^+]+{}^{ox}K_{a2}[H^+]+{}^{ox}K_{a1}\cdot{}^{ox}K_{a2}[H^+]^2)/({}^{red}K_{a1}[H^+] + {}^{red}K_{a2}[H^+]+{}^{red}K_{a1}\cdot{}^{red}K_{a2}[H^+]^2) \quad (1)$$

where E is the observed redox potential, E_0 is the redox potential of the protein in the alkaline extreme pH range, $[H^+]$ is the proton concentration, ${}^{ox}K_{ai}$ and ${}^{red}K_{ai}$ are the proton binding constants of the ith acid/base group in the oxidized and in the reduced state, respectively.

Acknowledgement

We wish to thank Profs. Bertini, Banci and Luchinat, for allowing us to collect NMR data at the Large Scale Facility CERM (University of Florence), and for helpful discussions, and Dr. Marco Trifuoggi for metal content analysis. We are also are grateful to Eka Chemicals AB for providing Kromasil HPLC columns, and to the Italian Ministry of University and Scientific research (PRIN 2000, 03185591) for financial supports.

[1] a) S. J. Lippard, J. M. Berg, *Principles of Bioinorganic Chemistry*, University Science Books, Mill Valley, CA, **1994**; b) R. H. Holm, P. Kennepohl, E. I. Solomon, *Chem. Rev.* **1996**, *96*, 2239–2314.

[2] a) K. D. Karlin, *Science* **1993**, *261*, 701–708; b) Y. Lu, S. M. Berry, T. D. Pfisterand, *Chem. Rev.* **2001**, *101*, 3047–3080.

[3] a) H. W. Hellinga, *Folding Des.* **1998**, *3*, R1–R8; b) W. F. DeGrado, C. M. Summa, V. Pavone, F. Nastri, A. Lombardi, *Annu. Rev. Biochem.* **1999**, *68*, 779–819; c) L. Regan, *Trends Biochem. Sci.* **1995**, *20*, 280–285; d) L. Baltzer, *Top. Curr. Chem.* **1999**, *202*, 39–75; e) D. A. Moffet, M. H. Hecht, *Chem. Rev.* **2001**, *101*, 3191–3203.

[4] a) F. Nastri, A. Lombardi, L. D. D'Andrea, M. Sanseverino, O. Maglio, V. Pavone, *Biopolymers* **1998**, *47*, 5–22; b) A. Lombardi, F. Nastri, V. Pavone, *Chem. Rev.* **2001**, *101*, 3165–3189.

[5] a) F. Nastri, A. Lombardi, G. Morelli, O. Maglio, G. D'Auria, C. Pedone, V. Pavone, *Chem. Eur. J.* **1997**, *3*, 340–349; b) G. D'Auria, O. Maglio, F. Nastri, A. Lombardi, M. Mazzeo, G. Morelli, L. Paolillo, C. Pedone, V. Pavone, *Chem. Eur. J.* **1997**, *3*, 350–362; c) F. Nastri, A. Lombardi, G. Morelli, C. Pedone, V. Pavone, G. Chottard, P. Battioni, D. J. Mansuy, *J. Biol. Inorg. Chem.* **1998**, *3*, 671–681; d) A. Lombardi, F. Nastri, M. Sanseverino, O. Maglio, C. Pedone, V. Pavone, *Inorg. Chim. Acta* **1998**, *275–276*, 301–313.

[6] a) A. Lombardi, C. M. Summa, S. Geremia, L. Randaccio, V. Pavone, W. F. DeGrado, *Proc. Natl. Acad. Sci. USA* **2000**, *97*, 6298–6305; b) A. Lombardi, D. Marasco, O. Maglio, L. Di Costanzo, F. Nastri, V. Pavone, *Proc. Natl. Acad. Sci. USA* **2000**, *97*, 11922–11927.

[7] a) D. R. Benson, B. R. Hart, X. Zhu, M. B. Doughty, *J. Am. Chem. Soc.* **1995**, *117*, 8502–8510; b) D. Liu, D. A. Williamson, M. L. Kennedy, T. D. Williams, M. M. Morton, D. R. Benson, *J. Am. Chem. Soc.* **1999**, *121*, 11798–11812; c) P. A. Arnold, D. R. Benson, D. J. Brink, M. P. Hendrich, G. S. Jas, M. L. Kennedy, D. T. Petasis, M. Wang, *Inorg. Chem.* **1997**, *36*, 5306–5315.

[8] a) P. A. Arnold, W. R. Shelton, D. R. Benson, *J. Am. Chem. Soc.* **1997**, *119*, 3181–3182; b) S. Sakamoto, A. Ueno, H. Mihara, *J. Chem. Soc. Perkin Trans. 2* **1998**, 2395–2404; c) S. Sakamoto, I. Obataya, A. Ueno, H. Mihara, *J. Chem. Soc. Perkin Trans. 2* **1999**, 2059–2069; d) M. M. Rosenblatt, D. L. Huffman, X. Wang, H. A. Remmer, K. S. Suslick, *J. Am. Chem. Soc.* **2002**, *124*, 12394–12395.

[9] a) H. K. Rau, W. Haehnel, *J. Am. Chem. Soc.* **1998**, *120*, 468–476; b) H. K. Rau, N. DeJonge, W. Haehnel, *Proc. Natl. Acad. Sci. USA* **1998**, *95*, 11526–11531; c) H. K. Rau, N. DeJonge, W. Haehnel, *Angew. Chem.* **2000**, *112*, 256–259; *Angew. Chem. Int. Ed.* **2000**, *39*, 250–253.

[10] a) D. E. Robertson, R. S. Farid, C. C. Moser, J. L. Urbauer, S. E. Mulholland, R. Pidikiti, J. D. Lear, A. J. Wand, W. F. DeGrado, P. L. Dutton, *Nature* **1994**, *368*, 425–432; b) J. M. Shifman, C. C. Moser, W. A. Kalsbeck, D. F. Bocian, P. L. Dutton, *Biochemistry* **1998**, *37*, 16815–16827; c) J. M. Shifman, B. R. Gibney, R. E. Sharp, P. L. Dutton, *Biochemistry* **2000**, *39*, 14813–14821; d) B. R. Gibney, P. L. Dutton, *Protein Sci.* **1999**, *8*, 1888–1898.
[11] J. W. Bryson, S. F. Betz, H. S. Lu, D. J. Suich, H. X. Zhou, K. T. O'Neil, W. F. DeGrado, *Science* **1995**, *270*, 935–940.
[12] J. W. Buchler in *The Porphyrin, Vol. 1* (Ed.: D. Dolphin), Academic Press, New York, **1979**, pp. 389–483.
[13] a) A. W. Johnson, I. T. Kay, *J. Chem. Soc.* **1960**, 2979–2983; b) M. Momenteau, D. Lexa, *Biochem. Biophys. Res. Commun.* **1974**, *58*, 940–944; c) R. Bonnet, M. J. Dimsdale, *J. Chem. Soc. Perkin Trans. 1* **1972**, 2540–2548.
[14] M. L. Kennedy, S. Silchenko, N. Houndonougbo, B. R. Gibney, P. L. Dutton, K. R. Rodgers, D. R. Benson, *J. Am. Chem. Soc.* **2001**, *123*, 4635–4636.
[15] P. Luo, R. L. Baldwin, *Biochemistry* **1997**, *36*, 8413–8421.
[16] J. Jeener, B. H. Meier, P. Backman, R. R. Ernst, *J. Chem. Phys.* **1979**, *71*, 4546–4553.
[17] A. Bax, D. G. Davis, *J. Magn. Reson.* **1985**, *65*, 355–360.
[18] U. Piantini, O. W. Sorensen, R. R. Ernst, *J. Am. Chem. Soc.* **1982**, *104*, 6800–6801.
[19] K. Wüthrich, *NMR of Proteins and Nucleic Acids*, Wiley, New York, **1986**.
[20] D. S. Wishart, B. D. Sikes, F. M. Richards, *J. Mol. Biol.* **1991**, *222*, 311–333.
[21] R. D. Guiles, J. Altman, I. D. Kuntz, L. Waskell, *Biochemistry* **1990**, *29*, 1276–1289.
[22] R. Santucci, C. Bongiovanni, S. Marini, R. Del Conte, M. Tien, L. Banci, M. Coletta, *Biochem. J.* **2000**, *349*, 85–90.
[23] a) V. Palaniappan, D. F. Bocian, *Biochemistry* **1994**, *33*, 14264–14274; b) M. Coletta, H. Costa, G. De Sanctis, F. Neri, G. Smulevich, D. L. Turner, H. Santos, *J. Biol. Chem.* **1997**, *272*, 24800–24804.
[24] S. Vuilleumier, M. Mutter, *Biopolymers* **1993**, *33*, 389–400.
[25] M. Nakano, H. Iwamaru, T. Tobita, *Biopolymers* **1982**, *21*, 805–815.
[26] J. S. Valentine, R. P. Sheridan, L. C. Allen, P. C. Kahn, *Proc. Natl. Acad. Sci. USA* **1979**, *76*, 1009–1013.
[27] a) H. Bang, J. O. Edwards, J. Kim, R. G. Lawler, K. Reynolds, W. J. Ryan, D. A. Sweigart, *J. Am. Chem. Soc.* **1992**, *114*, 2843–2852; b) M. Nakamura, A. Ikezaki, *Chem. Lett.* **1995**, 733–734; c) C. J. Medforth, C. M. Muzzi, K. M. Shea, K. M. Smith, R. J. Abraham, S. Jia, J. A. Shelnutt, *J. Chem. Soc. Perkin Trans. 2* **1997**, 833–837.
[28] A. Feis, M. P. Marzocchi, M. Paoli, G. Smulevich, *Biochemistry* **1994**, *33*, 4577–4583.
[29] J. D. Winefordner, *A Practical Guide to Graphite Furnace Atomic Absorption Spectrometry, Chemical Analysis, Vol. 149*, Wiley, NY, **1998**.
[30] D. Marion, K. Wüthrich, *Biochem. Biophys. Res. Commun.* **1983**, *113*, 967–974.
[31] F. Delaglio, S. Grzesiek, G. W. Vuister, G. Zhu, J. Pfeifer, A. Bax, *J. Biomol. NMR* **1995**, *6*, 277–293.
[32] C. Bartels, T. Xia, M. Billeter, P. Guntert, K. Wüthrich, *J. Biomol. NMR* **1995**, *5*, 1–10.
[33] S. Barlow, A. L. Rohl, S. Shi, C. M. Freeman, D. O'Hare, *J. Am. Chem. Soc.* **1996**, *118*, 7578–7592.

Received: February 10, 2003 [F4831]